INORGANIC CHEMISTRY
FRONTIERS

RESEARCH ARTICLE

View Article Online
View Journal | View Issue

Cite this: *Inorg. Chem. Front.*, 2025, **12**, 658

Facile one-pot synthesis of high-purity sodium antimony chalcogenides in polar solvents†

Saeed Ahmadi Vaselabadi, Brynn Benham and Colin A. Wolden *

Alkali metal chalcogenides have emerged as a new class of inorganic materials with diverse applications in energy conversion and storage owing to their structural versatility and wide range of properties. Strategies are needed for simple and cost-efficient synthetic approaches that enable the composition and functional properties of these materials to be systematically tuned. Herein, we present a novel wet-chemistry approach to produce ternary Na-based metal chalcogenides with varying compositions. Phase-pure Na_3SbCh_4 (Ch = S, Se) solid-state electrolytes are synthesized in a single-step fashion by reacting an ethanolic solution of Na chalcogenides with appropriately selected metal halides at room temperature. This process simplifies the reaction protocols, improves yield, and decreases the raw material loss incurred in multistep systems by eliminating the need for phase-pure binary metal chalcogenides. The reaction mechanisms and impurity profile of various sodium metal chalcogenides introduced in this work were methodically investigated through characterization techniques such as X-ray diffraction (XRD) and Raman spectroscopy. Among the chalcogenides, synthesis of the sulfide compounds (~99 wt% purity) was straightforward, achieving a yield of 92–95% whereas the selenides required more control to generate the appropriate mix of precursors, which resulted in a lower yield of 74–79% but with a high purity of 97.5–99.6 wt%. Electrochemical impedance spectroscopy of as-synthesized Na_3SbCh_4 (Ch = S, Se) showed a high ionic conductivity of 0.17–0.38 mS cm^{-1} and low activation energy of 0.19–0.21 eV comparable with other reports of solution-based synthesis. The one-pot scheme was successfully extended to the $NaSbCh_2$ (Ch = S, Se) system, producing phase pure ternary sodium metal chalcogenides with tunable band gaps (1.6–1.8 eV) appropriate for solar energy conversion applications. The "one-pot" approach offers a simple yet economical route for scalable production of bulk sodium ternary chalcogenides at ambient conditions.

Received 18th November 2024,
Accepted 29th November 2024

DOI: 10.1039/d4qi02941k

rsc.li/frontiers-inorganic

Introduction

Chalcogenides are essential classes of materials that include at least one chalcogen atom (Ch = S, Se, Te) in a reduced state. Unlike oxides, chalcogenides can form Ch–Ch bonds. Synthesis of a variety of chalcogenides is possible due to the reactivity of chalcogen anions with organic and inorganic cations such as alkali metals.[1–4] Alkali metal chalcogenides have recently been the focus of intense research as a new class of inorganic materials for the energy conversion and storage sector. They have been explored extensively in various applications such as photovoltaics, thermoelectric, optoelectronics, and energy storage.[1,5–8]

In this class of materials, slight differences in the elemental constitution, composition, and structure lead to different properties. For instance, sodium chalcogenides with Na_3PnCh_4 (Pn = P, Sb, As; Ch = S, Se) formula and their doped derivatives are being pursued as solid-state electrolytes for sodium-ion batteries due to their intrinsic high ionic conductivity and mechanical ductility. Originally based on sodium thiophosphate, Na_3PS_4, this class of solid-state electrolytes consists of polyanion polyhedra, *i.e.* $SbCh_4$,[3] with mobile Na^+ distributed in interstices and form a crystalline structure in either cubic phase ($I\bar{4}3m$ space group symmetry) or tetragonal phase with $P\bar{4}21c$ symmetry.[9–15] As an example of the diversity of this class of materials, ternaries with the stoichiometric variation $APnCh_2$ (A = Na, Li; Pn = Sb, Bi; Ch = S, Se) have received attention for their promising optical[16–21] and thermoelectric[5,22–24] properties. Specifically, they offer direct bandgaps suitable for solar light absorption, providing an abundant and environmentally friendly alternative.[6,20]

A variety of multinary chalcogenides have been synthesized through classic solid-state synthesis with the direct reaction of pure elements or binary precursors at high temperatures. This method is generally time-intensive due to the slow diffusion of

Chemical and Biological Engineering, Colorado School of Mines, Golden, Colorado 80401, USA. E-mail: cwolden@mines.edu

† Electronic supplementary information (ESI) available. See DOI: https://doi.org/10.1039/d4qi02941k

solid reactants and requires extremely high temperatures in air-free media like evacuated quartz ampoules. In addition, the products are limited to the most stable phases neglecting a diverse range of metastable phases only accessible at low temperatures.[1,6] Alternatively, alkali metal chalcogenide or polychalcogenide fluxes have been employed at milder temperatures. However, the underlying mechanism in these systems is quite underexplored. Moreover, from the scale-up standpoint, this method requires high operational complexity, equipment maintenance, and safety considerations addressing the toxic gas releases with molten salt handling.[25]

Solution-based approaches, such as colloidal hot injection and solvothermal hydrothermal methods, have been widely utilized in synthesizing ternary alkali chalcogenides requiring a low-to-medium temperature range at near- and supercritical conditions.[26] The colloidal method requires high boiling point solvents at elevated temperatures, and the products are usually contaminated with organic residues. Nanocrystalline alkali metal ternary I–V–VI_2 materials are typically synthesized using colloidal hot-injection that facilitates control over nucleation and growth of nanomaterials however suffer from costly and toxic precursors as well as non-volatile solvents that are hard to fully remove.[5,20,23]

On the other hand, solvo/hydrothermal methods involve the production of chalcogenides at high pressure and temperature in an autoclave. This method has been used to synthesize alkali metal chalcogenides such as $NaBiS_2$,[27–29] $AInS_2$ (A = Na, K),[30] $NaFeS_2$ [31] at temperatures ranging from 180–200 °C for extended periods (24–72 h), which utilized various chalcogen sources such as thiourea, L-cysteine, $Na_2S{\cdot}9H_2O$, and NaOH.

Overall, the liquid-phase synthetic approaches for multinary chalcogenides like Na_3SbCh_4 and $NaSbCh_2$ are often costly and limited in scalability due to equipment and raw material (precursor and solvent) requirements. Inspired by the simple solvothermal reaction of Na chalcogenides such as Na_2S with $InCl_3{\cdot}4H_2O$ in ethanol,[30,32] we present a simple wet-chemical synthesis method for sodium ternary chalcogenides at room temperature. This approach is built on the hypothesis that the synthesis of the binary and ternary metal chalcogenides could be simplified to a single step, where precursors derived from the binary reaction are directly utilized to fabricate ternary Na-based chalcogenides. This approach, specifically, simplifies the current reaction protocols for Na_3SbCh_4 and $NaSbCh_2$ by decreasing the raw material loss and improving the yield. The appropriate selection of precursors and solvents, as well as the impact of reaction parameters such as concentration and basicity, are investigated to optimize product purity.

First, we start by demonstrating the applicability of Na chalcogenide binary reagents to drive the single-step reaction with appropriate antimony salts in generating 314 chalcogenides with Na_3SbCh_4 (Ch = S, Se) stoichiometry in polar solvents. We further confirm their potential as solid-state electrolytes for sodium all-solid-state batteries. We then extend the same methodology to the 112 ternary compositions, *i.e.* $NaSbCh_2$ (Ch = S, Se), confirming their semiconductor character with photoabsorption studies. The underlying chemistry and impurity profile of various compositions were investigated systematically through a complementary set of characterization techniques including scanning electron microscopy (SEM), X-ray diffraction (XRD), and Raman spectroscopy.

Experimental methods

Materials

Sodium sulfide hydrate ($Na_2S{\cdot}xH_2O$, 60 wt%, Sigma-Aldrich), antimony(III) chloride ($SbCl_3$, ACS, 99% min, Alfa Aesar), antimony(III) bromide ($SbBr_3$, 99.5% metal basis, Thermo Scientific Chemicals), bismuth(III) bromide ($BiBr_3$, >98%, Sigma-Aldrich), sodium borohydride ($NaBH_4$, >98%, Sigma-Aldrich), sulfur (S, 99.999% trace metal basis, Thermo Scientific Chemicals), sodium (Na, Sigma-Aldrich), sodium hydroxide (NaOH, 98%, Thermo fisher scientific), selenium (Se, 99.99%, UMC), ethanol (EtOH, anhydrous, ≥99.5%, Sigma-Aldrich), dimethyl sulfoxide (DMSO, ACS, 99.9% min, Alfa Aesar), sodium selenate (Na_2SeO_4, anhydrous, 99.8+% metals basis, Thermo Scientific Chemicals), barium sulfate ($BaSO_4$, 99%, precipitated, Alfa Aesar), and UHP grade argon (Ar, 99.999%, General Air) were used as received without purification. Se pellets were further ground using a mortar and pestle to reduce particle size. All procedures were carried out in an Ar-filled glovebox (<5 ppm of H_2O) unless otherwise stated.

Synthesis

Na_3SbS_4. First, $Na_2S{\cdot}xH_2O$ hydrate flakes (60 wt%, Sigma) were purified as reported previously.[33] In this process, the low-grade Na_2S was dehydrated by heating the ground powder under vacuum at 70 °C (12 h) and 150 °C (12 h), consecutively. The dehydrated Na_2S was further purified by reducing the polysulfide and oxy-sulfide impurities at 600 °C under 50% H_2/Ar gas flow for 12 h in a packed bed setup. To prepare the chloride-based Na_3SbS_4, stoichiometric quantities of Na_2S (351 mg, 4.5 mmol), $SbCl_3$ (342 mg, 1.5 mmol), and S (48.1 mg, 1.5 mmol) were added to 10 ml of MeOH or DMSO and stirred overnight. The sample was recovered after decanting the solution and drying the precipitate at RT under vacuum overnight. Follow-up DMSO washes were carried out on the MeOH sample to remove the remaining NaCl byproducts. In the case of the bromide-based sample, Na_2S (234.2 mg, 3 mmol), $SbBr_3$ (361.5 mg, 1 mmol), and S (32.1 mg, 1 mmol) were added to 10 ml of EtOH and stirred overnight. The solution turned to a brown color after 1 hour of reaction. After overnight stirring, the sample was recovered by decanting and washing the precipitate with an excess of EtOH and drying under vacuum at RT (yield = ~92–95%). The sulfide was further dried at 150 °C under Ar to remove the remaining ethanol.

Na_3SbSe_4. To prepare the 0.4 M Se solution, 20% excess $NaBH_4$ (211.8 mg, 5.6 mmol) in 10 ml of EtOH was slowly added to Se (315.8 mg, 4 mmol) Se at RT to attain the "wine-red" solution (denoted as solution A) with no visible unreacted

Se grains (~4 h). Injecting excess $NaBH_4$ (~40%) generates a "clear" solution (solution B). Solutions A and B were separately used for the ternary reaction. $NaBH_4$ concentrations were 0.48 M and 0.56 M for A and B solutions, respectively. The selenide experiments were performed by adding corresponding quantities of NaOH (80, 160, 240, and 240 mg), and 5 ml solution of $SbBr_3$ (361.5, 361.5, 361.5, and 180.7 mg) in ethanol to the corresponding A and B solutions denoted as A/B4-1-2, A/B4-1-4, A/B4-1-6, and A/B8-1-12, respectively (Table 1). In all cases, the suspension turned dark instantly and changed to light brown after 1 day of stirring. The solutions were centrifuged, decanted, and washed with excess EtOH multiple times. The samples were collected by drying the precipitate at RT under vacuum overnight (yield = 74–79%). For the A/B8-1-12 samples, 180.7 mg (0.5 mmol) of $SbBr_3$ was used while keeping the [Se]/[NaOH] constant. The samples was further dried at 200 °C under Ar to remove the remaining solvated complexes. Supernatant from A4-2-6 and B4-2-6 samples are obtained after drying at 120 °C under Ar flow in a horizontal tube furnace.

The Na_3SbSe_4 reaction using Na_2Se_2 was attempted as follows: first, the Na_2Se_2 precursor solution was prepared as described previously.[34] In brief, 110 mg (4.78 mmol) of Na was dissolved in 10 mL EtOH for approx. 1 h to form sodium ethoxide (EtONa) solution. Next, we added 29.4 mg (0.78 mmol) of $NaBH_4$ to EtONa solution. In a three-neck flask, 430.6 mg (5.45 mmol) of Se was dispersed in 5 mL EtOH, and EtONa/$NaBH_4$ solution was dripped slowly in Se dispersion for approx. 1 h and let it react overnight to generate ethanolic Na_2Se_2 solution. The reaction with similar stoichiometry to the A/B4-1-6 experiment was conducted. First, 333.3 mg (8.33 mmol) of NaOH was added to the Na_2Se_2 solution. After 30 min of stirring, 494.6 mg (1.37 mmol) of $SbBr_3$ was added to the solution and the stirring continued overnight. A similar procedure was used to recover the sample powder as mentioned earlier (yield = ~70%.)

$NaSbS_2$. $SbBr_3$ powders (1 mmol) were added to 10 ml of EtOH to dissolve. After full dissolution, Na_2S (2 mmol) powders were slowly dropped into the halide solution causing an instantaneous color change. For samples with the basic agent, NaOH (5 mmol) was added before Na_2S addition. The obtained solutions after 1 day of reaction were decanted, and washed with excess EtOH until the supernatant became clear. The sample was dried under vacuum overnight to recover the sulfide. Extra grinding and washing with H_2O were performed to remove persistent NaBr impurities. Heat treatment at 300 °C was conducted in a horizontal tube furnace under flowing Ar (yield = ~70%).

$NaSbSe_2$. This experiment used 0.4 M clear Se solutions (B) as the activated Se source. Next, $SbBr_3$ and NaOH reagents were added with [Se] : [Sb] : [NaOH] = 2 : 1 : 2 molar ratios. Similar recovery and purification as other selenides were implemented to obtain $NaSbSe_2$ powder (yield = ~80%).

Material characterization

Simultaneous thermogravimetric analysis (TGA) and differential scanning calorimetry (DSC) were carried out on a TA Instruments SDT-Q600 model. For a typical run, 10 mg of sample was loaded into a pre-cleaned alumina pan and heated and cooled for one cycle under flowing Ar at 10 °C min^{-1} rate. X-ray diffraction (XRD) was performed with a Philips X'Pert X-ray diffractometer with Cu Kα radiation (λ = 0.15405 nm). Samples were prepared on a glass slide with protective tape covering the material to minimize air exposure. Rietveld refinement of the XRD patterns was conducted using the generalized structure analysis system (GSAS-II) software.[35] A WiTec alpha 300 M Confocal Microscope/Raman Spectrometer employing a 100 mW 532 nm laser was used to obtain Raman spectra. Samples were mounted on a glass slide and sealed under a 0.1 mm quartz cover slip. The laser was focused through the coverslip onto the sample using a 20× objective, and spectra were collected using a CCD detector (Andor Technologies) at −60 °C. Field emission scanning electron microscopy (FESEM) images were collected on a JEOL JSM-7000F FESEM instrument equipped with energy-dispersive X-ray spectroscopy (EDX) for compositional analysis. To prepare the samples for SEM and EDX measurements, powder samples were placed onto an aluminum stub using double-sided carbon tape. An accelerating voltage of 5 kV was used for taking the SEM image while a higher voltage of 15–20 V was employed for EDX spectra collection. ^{77}Se Nuclear Magnetic Resonance (NMR) spectroscopy was conducted on a JEOL ECA-500 500 MHz liquids-only spectrometer. A 1.5 M solution of sodium selenate (Na_2SeO_4) in D_2O was used as standard. Fourier transform infrared (FTIR) spectroscopy was carried out on a Nicolet Summit FT-IR spectrometer using an attenuated total reflection (ATR) acces-

Table 1 Summary of solution-phase synthesis of Na_3SbSe_4 reported in this work

Sample name	Se solution	Molar ratio [Se] : [Sb] : [NaOH]	Se conc. (M)	$NaBH_4$ conc. (M)	Sb conc. (M)	NaOH (M)	Product	Size (nm)
A4-1-2	A	4 : 1 : 2	0.4	0.48	0.1	0.2	$NaSbSe_2$ (72%), Na_3SbSe_4 (28%)	—
A4-1-4	A	4 : 1 : 4	0.4	0.48	0.1	0.4	Na_3SbSe_4 (90.8%), $NaSbSe_2$ (9.2%)	26.4
A4-1-6	A	4 : 1 : 6	0.4	0.48	0.1	0.6	Na_3SbSe_4 (99.3%), $NaSbSe_2$ (0.7%)	26.2
A8-1-12	A	8 : 1 : 12	0.4	0.48	0.05	0.6	Na_3SbSe_4 (99.6%), $NaSbSe_2$ (0.4%)	17.9
B4-1-2	B	4 : 1 : 2	0.4	0.56	0.1	0.2	$NaSbSe_2$ (56.6%), Na_3SbSe_4 (9.2%), NaBr (34.2%)	—
B4-1-4	B	4 : 1 : 4	0.4	0.56	0.1	0.4	$NaSbSe_2$ (<100%), unknown impurity	21.1
B4-1-6	B	4 : 1 : 6	0.4	0.56	0.1	0.6	Na_3SbSe_3 (~82%), Na_3SbSe_4 (~18%)	—
B8-1-12	B	8 : 1 : 12	0.4	0.56	0.05	0.6	Na_3SbSe_4 (97.5%), $NaSbSe_2$ (2.5%)	37.3

sory equipped with a diamond crystal (16 scans, absorption mode, 4 cm^{-1} resolution). All sample preparation was done in an Ar glovebox.

Electrochemical characterization

Pellets of Na_3SbCh_4 (Ch = S, Se) electrolytes were prepared for electrical conductivity measurement *via* conventional uniaxial pressing. For this purpose, 150–250 mg of the electrolyte was loaded into a 12 mm PEEK split cell with stainless steel plungers under a uniaxial fabrication pressure of 270 MPa and held for 5 min. Pellets were typically 0.6–0.8 mm thick. The pellets were contacted using stainless steel plungers as electrodes for electrochemical characterization. A Gamry Interface 1000E potentiostat was used to perform electrochemical impedance spectroscopy (EIS) measurements across a frequency range of 1 Hz to 1 MHz with a 10 mV perturbation with a stacking pressure of 75 MPa. Temperature-dependent EIS testing was performed by heating the split cell apparatus with an electrical heating element and allowing it to stabilize at the target temperature for 1.5 h. DC polarization measurements were conducted by applying multi-step potentials to the sample (04, 0.6, 0.8, and 1 V) and recording the transient current. The steady-state current was recorded after 2 h at each step potential, and the electrical conductivity was calculated using Ohm's law.

Optical absorption characterization

A Cary 5G UV-Vis and NIR spectrophotometer, with a 200–1500 nm range was used to obtain diffuse reflectance data. Barium sulfate ($BaSO_4$) was used as a reference with 100% reflectance. To prepare the samples, a 25 : 75% mixture of ternary powder and $BaSO_4$ was ground in a pestle and mortar and pelletized into 10 mm pellets. The pellets were loaded on an integrating sphere attachment on the UV-Vis instrument. The reflectance *versus* wavelength data were collected to obtain the direct and indirect bandgaps of $NaSbCh_2$ (Ch = S, Se) samples using the Kubelka–Munk transformation ($F(R)$) and Tauc plots (eqn (1) and (2)).[36,37]

$$F(R) = \frac{(1-R)^2}{2R} \quad (1)$$

$$(F(R)h\nu)^n \propto (h\nu - E_g) \quad (2)$$

R, h, ν, and E_g represent absolute reflectance, Planck's constant, light frequency, and band gap respectively. The value of constant n is equal to 2 for direct and $\frac{1}{2}$ for indirect band gap transitions.

Results and discussion

Na_3SbCh_4 (Ch = S, Se) synthesis and structural characterization

The main reagents commonly used to produce Na_3SbCh_4 are pure binary chalcogenides such as Na_2Ch and Sb_2Ch_3. As we have shown in our previous reports, Sb_2Ch_3 can be prepared through simple metathesis reactions.[11,12] However, the individual synthesis and purification of binary chalcogenides followed by their incorporation in ternary synthesis results in extensive raw materials loss and reductions in the overall reaction yield. Therefore, we submit a simplified protocol for the production and purification of Na_3SbCh_4 electrolytes by combining the binary and ternary reaction steps into a "one-pot" approach as illustrated in Fig. 1.

The choice of solvent is crucial in this process; first, the solvent must be able to dissolve all the precursors without any side reactions since this approach utilizes the products of the metathesis reaction as intermediates. Second, the solvent should facilitate the subsequent precipitation of the desired product with simple recovery steps based on the solubility criteria. Direct precipitation through filtration and centrifugation is typically more desirable compared to other energy-intensive solvent removal routines. Third, the reactants, products, and intermediates should be stable against solvents. Lastly, purification from the solvato complex should be attainable at low to moderate temperatures.

Sulfides

The standard solution-phase reaction of Na_3SbCh_4 is based on the nucleophilic attack of the chalcogenide ions on the binary compounds. In this approach, binary chalcogenides Sb_2Ch_3 are reacted with alkali metal polychalcogenides to form the salts of polyhedral anions of $[SbCh_4]^{3-}$. It is widely known that group (V) sulfides such as Sb_2S_3 dissolve in alkaline aqueous solutions to produce tetrahedral thiometallates in the form of $[SbS_3]^{3-}$. Furthermore, the addition of suitable cations can drive the formation of various polyanions in the presence of $[SbS_3]^{3-}$ species.[3] Previously, we utilized this concept by dissolving Sb_2S_3 in an alkaline solution of Na_2S in EtOH. Dissolution of alkali metal sulfides such as Li_2S and Na_2S in highly polar alcohols results in the formation of hydrosulfide and alkoxide ions through alcoholysis creating an alkaline solution.[32,38,39] The formed HS^- anions act as the driving force for the formation of intermediate Na_3SbS_3 in ethanolic solution, and its subsequent oxidation to Na_3SbS_4 (eqn (3) and (S1)–(S4)†). The redox reaction is based on coupling Sb oxi-

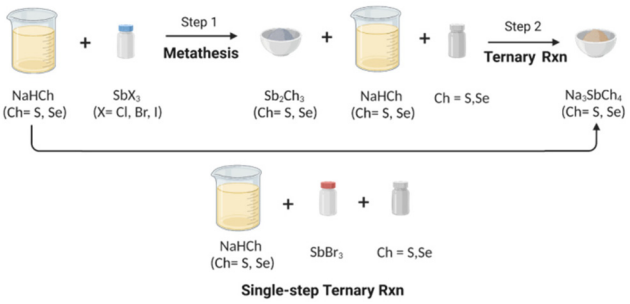

Fig. 1 Schematics comparing two-step and single-step ("one-pot") reaction for Na_3SbSCh_4 (Ch = S, Se) synthesis in ethanol (created with BioRender.com).

dation and sulfur reduction in ethanol. Sulfur solubility in ethanol further facilitates this reduction.

$$3Na_2S_{(sol)} + Sb_2S_{3(sol)} + 2S_{(sol)} \xrightarrow{EtOH} 2Na_3SbS_{4(s)} \quad (3)$$

The first approach to bypass the need for two binary precursors was to combine metathesis with ternary formation using methanol as the solvent and $SbCl_3$, the most inexpensive and widely available antimony halide (eqn (4)):

$$3Na_2S_{(sol)} + SbCl_{3(sol)} + S_{(sol)} \xrightarrow{MeOH} Na_3SbS_{4(sol)} + 3NaCl_{(sol)} \quad (4)$$

The reaction was successful, but since both products are highly soluble extensive washing with DMSO was required to recover phase pure Na_3SbS_4, making the approach expensive and inefficient. More details of the process and characterization are provided in the ESI (Fig. S1†).

This prompted us to search for other reagents and solvents that could resolve the NaCl separation issue. Interestingly, other halide precursors such as antimony bromide/iodide (SbX_3, X = Br, I) are very soluble in alcohols, and their reaction with Na chalcogenides reagents results in the formation of highly soluble Na halides (NaX). For instance, NaBr solubility in EtOH is 2.496 g per 100 g EtOH.[40] We previously showed that EtOH is a suitable solvent for ternary reaction since it improves overall ternary yield and retains comparable ionic conductivity to other synthetic approaches.[12] Hence, we hypothesized that the following reaction (eqn (5)) with $SbBr_3$ as the antimony source is thermodynamically favorable and could proceed in EtOH:

$$3Na_2S_{(sol)} + SbBr_{3(sol)} + S_{(sol)} \xrightarrow{EtOH} Na_3SbS_{4(s)} + 3NaBr_{(sol)} \quad (5)$$

Since Na_3SbS_4 is sparingly soluble in EtOH, this scheme provides direct precipitation of the sulfide at RT based on solubility criteria without any extra processing. The obtained powder was further dried at 150 °C to remove any remaining solvents. Fig. 2a shows the XRD patterns of powder collected at RT and after the 150 °C drying step. The crystal structure matches well with the tetragonal phase of Na_3SbS_4 ($P\bar{4}21c$ space group, PDF 04-023-8842). The Rietveld refinement of the RT sample (Fig. S2†) shows a 98.8 wt% purity for Na_3SbS_4 with a 1.2% secondary Na_3SbS_3 phase.

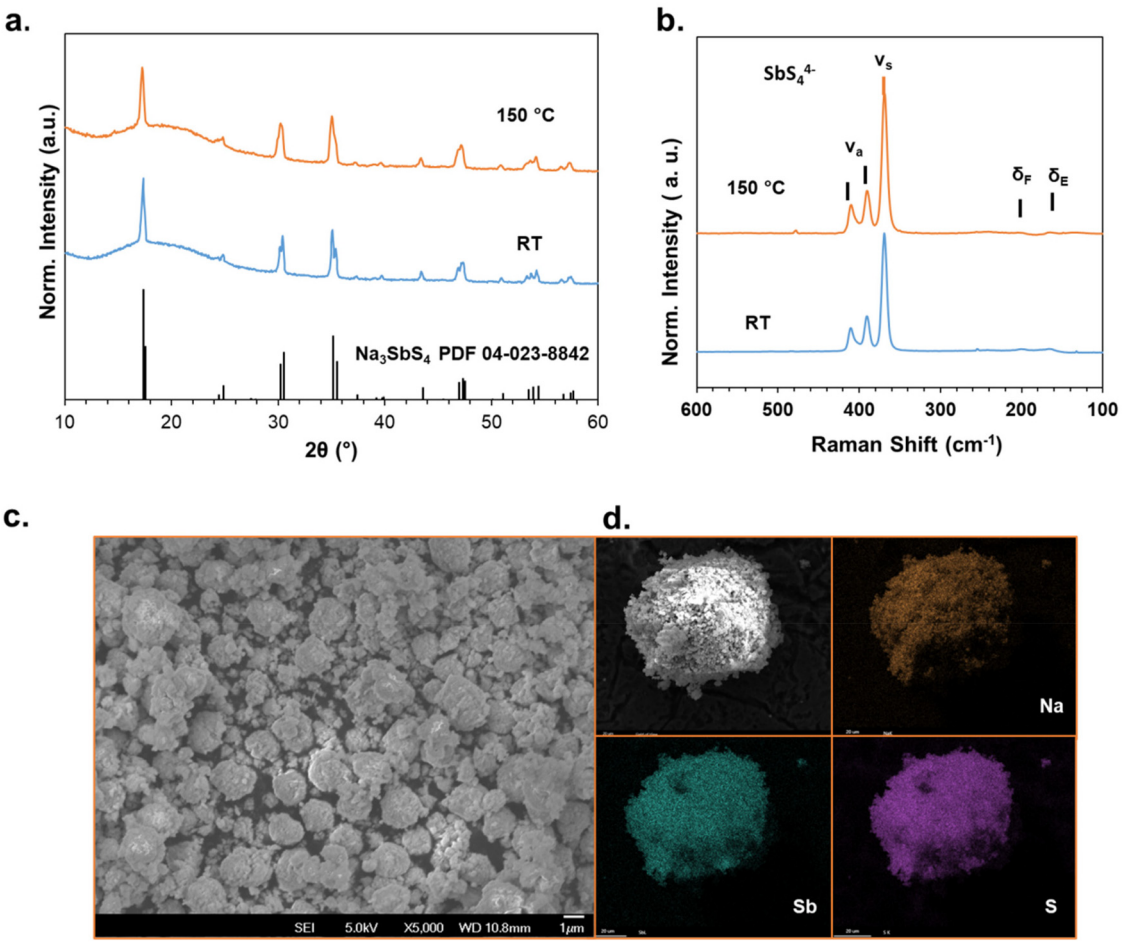

Fig. 2 (a) XRD patterns and (b) corresponding Raman spectra Na_3SbS_4 recovered from one-pot reaction bromide halide at RT and 150°. (c) SEM micrograph, and (d) EDAX elemental mapping of Na_3SbS_4 at RT.

The lattice parameters for Na_3SbS_4 ($a = b = 7.1736$ Å, $c = 7.3041$ Å, $V = 375.877$ Å^3) are in good agreement with the values reported from Na_3SbS_4 synthesized through other methods.[15,41] The average crystallite size of ~31.2 nm for the primary particle is calculated from the Scherrer equation. As expected, the supernatant contains pure NaBr further confirming the feasibility of a one-pot reaction with bromide salt (Fig. S3†).

Fig. 2b exhibits the Raman spectra of corresponding Na_3SbS_4 samples and confirms the presence of tetrathioantimonate anions (SbS_4^{4-}).[42] The SEM images of the RT sample (Fig. 2c) feature large crystals (~1–5 μm) that are formed through the agglomeration of primary nanoparticles. EDAX mapping confirms the homogeneity of the elemental constituents throughout the sample (Fig. 2d and S4†). FTIR spectroscopy (Fig. S5†) further demonstrated that mild heat treatment at 150 °C is required to remove residual solvents. In short, we showed that EtOH is an ideal solvent for this one-pot scheme that facilitates RT reactive precipitation of highly pure Na_3SbS_4 with high yield in a cost-effective and scalable approach.

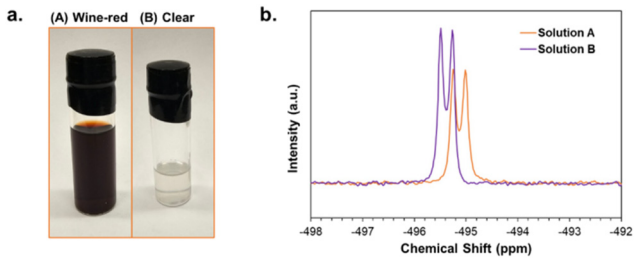

Fig. 3 (a) Photograph of activated Se solution used as Se precursors in Na_3SbSe_4 reactions, (b) ^{77}Se NMR spectra of Se solutions (A: wine-red, and B: clear solution).

Selenide

In our previous work, we presented a novel solution-based method to synthesize Sb_2Se_3 and Na_3SbSe_4 (314 phase) in polar solvents such as H_2O and EtOH utilizing sodium hydroselenide (NaHSe) solution as the main resource for activated Se.[11] In this process, elemental Se is reduced using $NaBH_4$ in EtOH to generate NaHSe reagent at RT (eqn (S5)†). Then, crystalline Sb_2Se_3 is recovered from the metathesis reaction between NaHSe and $SbCl_3$ followed by heat treatment at 300 °C (eqn (S6)†). Subsequently, Sb_2Se_3 is used as the precursor for the ternary reaction in conjunction with $NaHSe_{(sol)}$ and $Se_{(s)}$ reagents (eqn (6)).

$$3NaHSe_{(sol)} + Sb_2Se_{3(s)} + 3NaOH_{(sol)} + 2Se_{(s)} \rightarrow 2Na_3SbSe_{4(s)} + 3H_2O_{(l)} \quad (6)$$

Similar to the sulfide synthesis detailed earlier, we attempted a one-pot reaction using antimony bromide as the precursor assuming that the nucleophilic attack of the activated Se on the halide can generate the ternary selenides directly as suggested in eqn (7). The formation of sodium bromide, analogous to the sulfide reaction, facilitates the direct precipitation of the *t* at RT through centrifugation and supernatant removal.

$$4NaHSe_{(sol)} + SbBr_{3(sol)} + 2NaOH_{(sol)} \rightarrow Na_3SbSe_{4(s)} + 3NaBr_{(sol)} + 2H_2O + H_2 \quad (7)$$

In this reaction, EtOH serves multiple roles; first, the Se reduction with $NaBH_4$ has been successfully reported in H_2O and EtOH. However, the aqueous Se reduction is often

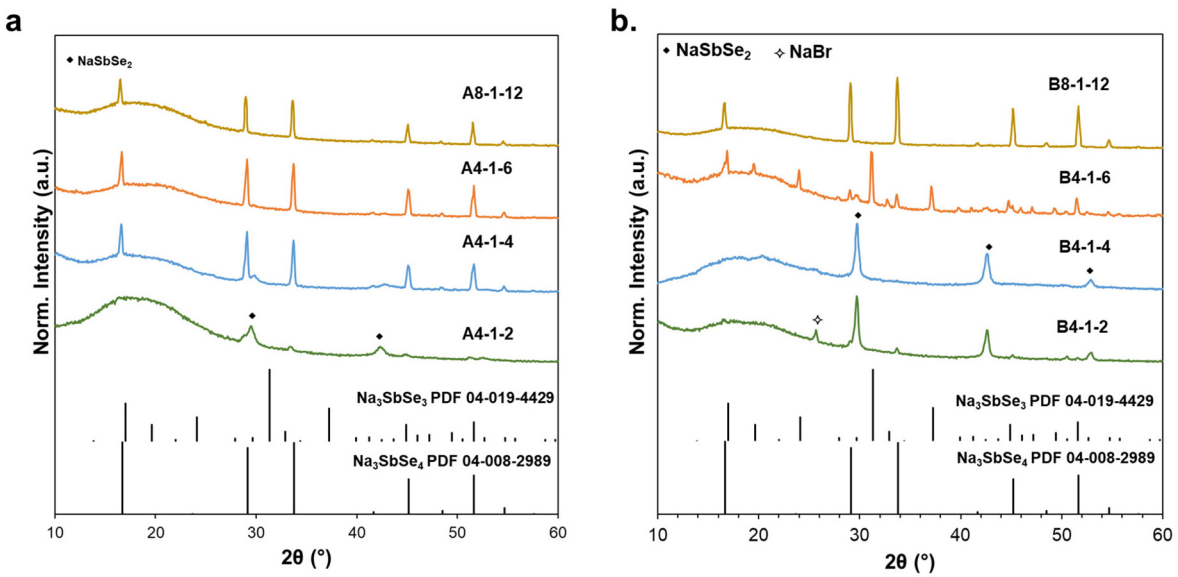

Fig. 4 XRD patterns of Na_3SbSe_4 one-pot reaction precipitate with (a) "wine-red" (A) solution, and (b) "clear" (B) solution with varying [Se] : [Sb] : [NaOH] compositions.

accompanied by the formation of borax as a side product, which contaminates the process. Additionally, 314 phase is soluble in H_2O further complicating its recovery. In this context, ethanol is the ideal solvent which also facilitates the reactive precipitation of the desired 314 phase during the final stage of reaction. Second, $NaBH_4$ is moderately soluble in EtOH which leads to a slow decomposition and little loss of $NaBH_4$, thereby preserving its effectiveness as a reducing agent over time.[43] Third, Se reduction in ethanol produces a mildly alkaline environment contributing to the basicity needed to enhance the solubility of $[SbCh_x]$ intermediates (eqn (8)).[3,44]

$$Se_{(s)} + NaBH_{4(sol)} + 3C_2H_5OH_{(l)} \rightarrow NaHSe_{(sol)} + B(OC_2H_5)_3 + 3H_{2(g)} \quad (8)$$

Furthermore, it was found that the state of the NaHSe reagent impacted the reaction pathways. Initially, the expected "clear" solution[44] was formed upon dropwise addition of $NaBH_4$ solution (20% excess) to the Se suspension indicating the full reduction of Se after 1 h; however, the solution started to slowly turn light wine-red with color darkening as the stirring continued. Previous studies utilizing aqueous NaHSe have reported that the initial "clear" solution turns "wine-red" possibly due to its reactivity with water. The red color is attributed to the presence of amorphous selenium and polyselenide species in the solution.[45,46] We observed similar behavior in ethanolic NaHSe solution even though the reaction was carried out in a glove box with minimal H_2O (<5 ppm). Alternatively, injecting additional $NaBH_4$ reverts the solution's state to "clear". De Oliviera *et al.*[47] also reported the occurrence of wine-red color and its reversibility upon adding excess $NaBH_4$. They identified various Se species through organoselenide reactions involving reduced Se in ethanol and benzyl chloride. They concluded that by tuning the ratio of $NaBH_4$ to Se, alternating concentrations of HSe^- and Se_2^{2-} species trapped through an alkylation reaction with benzyl chloride could be generated and identified *via* NMR studies. NMR is very suitable for characterizing the various Se species in solutions owing to the Se NMR active spin isotope.[47–50]

Similarly, we conducted ^{77}Se NMR of the ethanolic Se solution to further understand the nature of the color change in the Se solution (Fig. 3). We prepared two Se solutions in ethanol for this experiment as detailed in the Experimental section (Fig. 3a). In the first solution (A), the Se was reduced with a 20% excess solution of $NaBH_4$ in EtOH, generating a wine-red solution after 4 h. Small aliquots were separated for NMR analysis. The second solution (B) was prepared by titrating $NaBH_4$ in solution A until the solution became "clear". The Se concentration was maintained at 0.4 M for A and B solutions while $NaBH_4$ concentrations were adjusted to 0.48 M and 0.56 M for A and B, respectively.

The observed doublet peak at −495 ppm in the NMR profile for solutions A and B is in very good agreement with previous reports assigning it to HSe^- monoselenide anion (Fig. 3b).[47,50]

The small shift to a lower chemical shift for solution B is possibly due to a slight change in the solvated environment ($[B]_{NaBH_4}$ = 0.56 M *vs.* $[A]_{NaBH_4}$ 0.4 M), and the higher intensity of NMR signals for "clear" solution indicates a slightly higher concentration of HSe^{-1}. Nevertheless, neither solution shows signs of other selenium species such as Se^{2-} and Se_2^{2-} anions. Cusick and Dance[49] reported that they could not find any evidence of Se_2^{2-} in the NMR spectrum of Na_2Se_2 in ethanol, since most probably it dissociates to HSe^- and $(Se_x)^{2-}$ or $Se_{(s)}$ species. Also, the diselenide Se_2^{2-} is reported to be highly unstable while exposed to ambient oxygen and decomposes to monoselenide (Se^{2-}) and $Se_{(s)}$.[51,52] From these findings and our observation of the color shift in ethanolic Se, we can assume that the initial wine-red color is due to the formation of amorphous Se from Na_2Se_2 decomposition while most of the activated Se species are in form of HSe^{-1}. The addition of extra $NaBH_4$ further reduces the $Se_{(s)}$ and increases HSe^{-1} concentration reclaiming the clear solution. It is not feasible to conclusively pinpoint the water moisture (eqn (S8) and (S9)†) or oxygen (eqn (S10)†) as the source of decomposition and

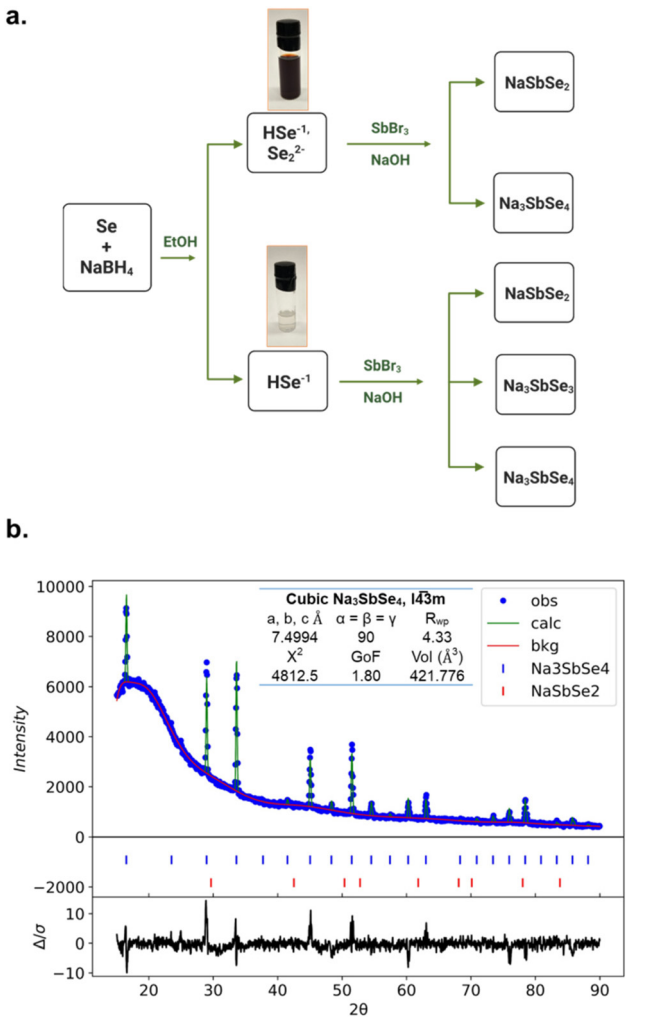

Fig. 5 (a) Schematics of ethanolic Se species and ternary selenide products from "one-pot" approach. (b) Rietveld refinement of Na_3SbSe_4 sample recovered from A8-1-12 experiment.

color shift in the Se solution. Despite the color shift, the concentration of activated Se in either state is constant; however, we can conclude that the monoselenide (HSe^{-1}) is the highly dominant species in both solutions while appreciable amounts of unstable Se_2^{2-} exist in the "wine-red" solution (A).

To systematically study the impact of color shift and reactant concentration, we designed a series of experiments with solutions A and B as the source of Se species and varying concentrations of Se and NaOH solutions. Fig. 4 compares XRD patterns of the one-pot reaction precipitate using (a) the wine-red and (b) clear NaHSe solutions. All powders were recovered at RT under vacuum without any post-synthesis heat treatment. The first set of reactions varied the NaOH concentration while fixing the [Se] : [Sb] ratio at 4 : 1. Our initial experiment was based on the stoichiometry shown in eqn (7) in which the concentration ratio of the precursors was [Se] : [Sb] : [NaOH] = 4 : 1 : 2. At this condition both solutions primarily generated $NaSbSe_2$ (112 phase). Considering the Sb_2Se_3 as the intermediate formed in this scheme (eqn (S6)†), we can assume that hydrobromic acid (HBr) is also generated. Therefore, excess NaOH is required to neutralize the intermediate acid and maintain the basic condition required to drive the 314 phase reaction. In the case of the wine-red reagent increasing the NaOH ratio to 4 produced primarily Na_3SbSe_4, and further increasing to 6 eliminated the 112 phase (A4-1-6).

In contrast, with solution B the 112 phase persisted as NaOH was increased to 4, and at 6 the reaction produced a mixture of the 313 and 314 ternaries (B4-1-6). Optimization showed that the desired 314 phase could also be achieved through the use of excess Se. In this case the [Se] : [Sb] ratio was doubled to 8 : 1, and the [NaOH] : [Se] ratio was fixed to maintain solution pH and for consistency. Both solutions produced predominantly 314 with trace levels of the 112 phase, however slightly better purity was obtained with wine-red solution. Table 1 also summarizes all the reaction parameters, product composition as well as crystalline size determined from the Scherrer equation.

Although the purity of Na_3SbSe_4 for both A8-1-12 and B8-1-12 reactions was very similar, solution A proved superior in terms of reactant concentration and yield; in the case of A4-1-6, solution A produced comparable purity with a higher yield and lower Se concentration compared to reactions with solution B (B8-1-12 and B4-1-6). The prevalence of solution A was attributed to the presence of diselenide salts, and characterization of the supernatant showed that the Na_2Se_2 signal is more significant from the wine-red Se solution (A) further confirming our hypothesis (Fig. S6†). These results highlighted that reactions with solution (A), that included a mixture of activated Se species in the form of monoselenide and diselenide, proved to be favorable toward the production of the Na_3SbSe_4 phase with minimal quantities of precursors required. Another important observation was the absence of any gas evolution, which suggested that the proposed synthesis reaction (eqn (7)) is not correct. Based on our findings we propose that the presence of both NaHSe and selenide precursors promotes Na_3SbSe_4 formation:

$$2NaHSe_{(sol)} + SbBr_{3(sol)} + Na_2Se_{2(sol)} + 2NaOH_{(sol)} \rightarrow Na_3SbSe_{4(s)} + 3NaBr_{(sol)} + 2H_2O_{(l)} \quad (9)$$

It is proposed that insufficient selenide leads to the formation of the 313 phase through eqn (10):

$$3NaHSe_{(sol)} + SbBr_{3(sol)} + 3NaOH_{(sol)} \rightarrow Na_3SbSe_{3(s)} + 3NaBr_{(sol)} + 3H_2O_{(l)} \quad (10)$$

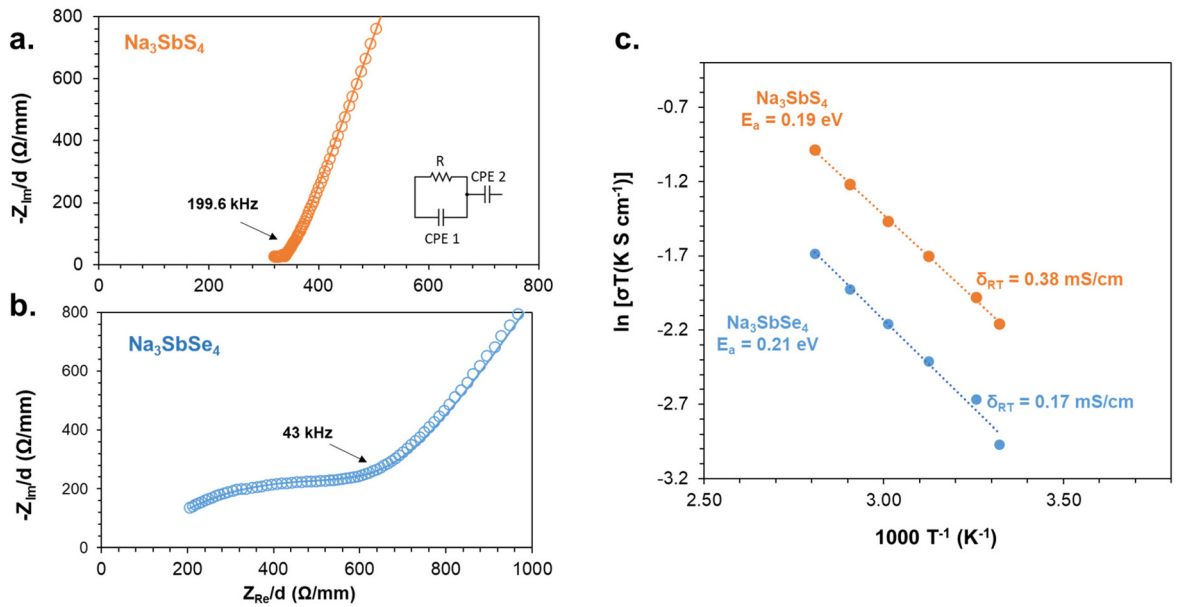

Fig. 6 Nyquist plots of (a) Na_3SbS_4, (b) Na_3SbSe_4, and (c) Arrhenius plot of ternary chalcogenides obtained from temperature-dependent impedance spectroscopy. The samples are recovered from the one-pot reaction in EtOH at RT.

Finally, insufficient NaOH to neutralize the released HBr results in the formation of the 112 ternary through eqn (11):

$$2NaHSe_{(sol)} + SbBr_{3(sol)} + 2NaOH_{(sol)} \rightarrow NaSbSe_{2(s)} + 3NaBr_{(sol)} + 2H_2O_{(l)} \quad (11)$$

In studies on similar ternary chalcogenides, such as Cu_3SbS_4, it has been shown that a basic environment and the presence of oxidizing agents, like elemental chalcogens, are crucial for the oxidation of Sb(III) to Sb(V). This emphasizes the importance of additional sulfur in the Na_3SbS_4 reaction and the necessity of excess Se and NaOH in the selenide analog, Na_3SbSe_4.[32,53] Schematics of possible Se species formed in ethanolic Se precursor solution and their subsequent products in the proposed one-pot reaction are depicted in Fig. 5a. Additional data supporting these conclusions is included in the ESI (Fig. (S7)–(S9)†).

Fig. 5b shows the Rietveld refinement of the Na_3SbSe_4 sample recovered from the A8-1-12 experiment. The dominant crystalline phase (99.6 wt%) is cubic Na_3SbSe_4 with I_Q3m space group as the typical high-temperature polymorph in Na_3SbCh_4 structure type. In this structure, the $SbSe_4$ polyanion forms a body-centered sublattice with Na ions positioned in the octahedral voids (Fig. S10†).[54] The sulfide counterpart forms the low-temperature tetragonal phase with the $P\bar{4}21c$ space group with slight changes in polyhedra and Na positions (Fig. S10†). A small trace of $NaSbSe_2$ (0.4 wt%) is also identified in the compound. SEM image and EDAX mapping of this sample is shown in Fig. S11.† Similar to the sulfide case, a mild heat treatment is carried out to remove any residual complexated solvents from Na_3SbSe_4 as demonstrated by the IR spectra in Fig. S12.†

Transport properties

The ionic transport of the ternary chalcogenides was characterized using electrochemical impedance spectroscopy (EIS). Fig. 6a and b shows representative room temperature Nyquist plots of Na_3SbCh_4 recorded from the one-pot reaction products. The impedance spectrum is fitted with an R-CPE element for the bulk resistance added to the CPE element contributing to the electronic resistance of the blocking electrodes (Table S1†). The ionic conductivity is calculated from the obtained resistance in the Nyquist plots. The ionic conductivity of Na_3SbS_4 (0.38 mS cm^{-1}) and Na_3SbSe_4 (0.17 mS cm^{-1}) from the one-pot reaction recovered at RT are in good agreement with our previous work utilizing the standard "two-pot" solution approach (Table S3†).[11,12]

The kinetics of Na^+ transport was studied *via* temperature-dependent EIS. The activation energy, derived from Arrhenius plots (Fig. 6c), shows almost identical values for both sulfides and selenides comparable with other reports in the literature.[54–57] Even though a more facile ionic transport in selenide composition is predicted due to lattice expansion and softening,[54] we see a lower ionic conductivity for selenide which is attributed to the presence of off-stoichiometry and impurity phases. The as-synthesized Na_3SbS_4 and Na_3SbSe_4 contain trace quantities of low-conductive Na_3SbS_3 and $NaSbSe_2$ compounds, respectively, along with residual organic impurities. Furthermore, they possess lower crystallinity than highly crystalline chalcogenides developed from classical solid-state reactions, which may contribute to their inferior ionic conductivity (Table S3†).

DC polarization measurements were carried out to determine electronic conductivity. Fig. S13† shows the transient

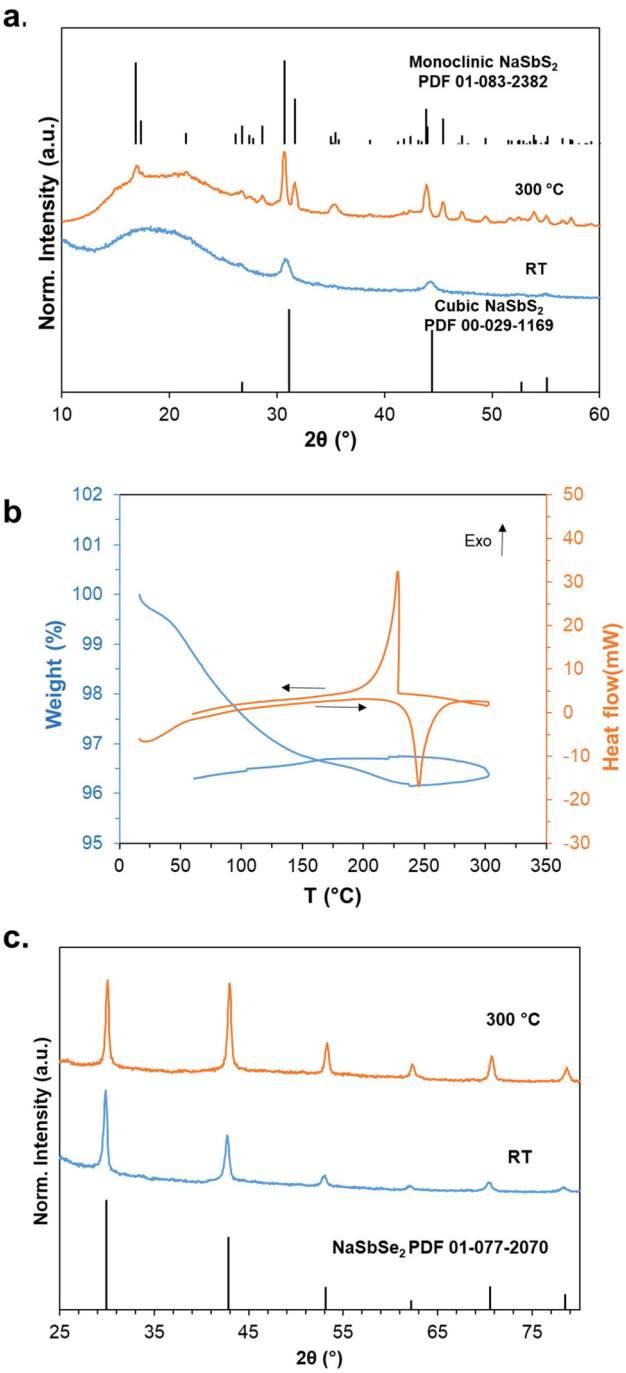

Fig. 7 (a) XRD patterns of $NaSbS_2$ before and after annealing at 300 °C. (b) TGA-DSC scans of cubic $NaSbS_2$ recovered at RT. (c) XRD patterns of $NaSbSe_2$ recovered at RT and annealed at 300 °C.

current time for sulfide and selenide at 0.6 V indicating the lower electronic conductivity obtained for ternary sulfide most likely due to different $NaSbCh_2$ impurity concentrations. The obtained values from Ohm's law are 1.22×10^{-6} mS cm^{-1} and 2.11×10^{-5} mS cm^{-1} for Na_3SbS_4 and Na_3SbSe_4, respectively. The recorded ionic conductivity of ternary chalcogenides is 5–6 orders of magnitude higher than the electronic conductivity demonstrating the ideal characteristics of superionic conductors.

$NaPnCh_2$ (Pn = Sb, Bi, Ch = S, Se) synthesis and structural characterization

Stoichiometric variation provides different functionalities in ternary alkali metal chalcogenides. For instance, $NaSbCh_2$ materials, another variant composition of Na_3SbCh_4, are considered mixed ionic-electronic conductors with low band gaps, making them promising candidates for semiconductor applications. Conversely, they lack the superionic tendency of the latter composition largely due to an absence of Na-ion diffusion pathways in the lattice structure and a difference in their density of states. $NaPnCh_2$ typically crystallizes with a disordered rock-salt cubic structure in which Na^+/Sb^{3+} cations are positioned on the octahedral sites in a face-centered arrangement of chalcogenide ions, but other stable crystallographic structures like monoclinic and triclinic have also been reported.[5,6,19–21]

Inspired by the side product formed in Na_3SbCh_4 synthesis, we turned to directly synthesizing $NaSbCh_2$. Eqn (12) exhibits the simple scheme for the alkali metal sulfides:

$$2Na_2S + PnBr_3 \rightarrow NaSbS_2 + 3NaBr \quad (Pn = Bi, Sb). \qquad (12)$$

This scheme was first tested using $SbBr_3$ as the pnictogen precursor in ethanol. The XRD patterns of the precipitate recovered at RT (Fig. 7a) show a cubic phase of $NaSbS_2$ ($Fm\bar{3}m$ space group) with broad peaks indicating the nanocrystalline nature of the primary particles (Fig. 7a). Heat treatment was carried out to remove any remaining solvated complexes and crystallize any possible amorphous phases. Interestingly, the initial cubic phase transitioned to a monoclinic ($C2/c$) phase after annealing at 300 °C. The thermal analysis of the sample obtained at RT through DSC also confirms the occurrence of a structural change at 245 °C (Fig. 7b). Raman spectra further verify this phase transition (Fig. S14†). Xia *et al.* reported a similar phase transition induced by heat treatment.[58]

The polymorphism in $NaSbS_2$ is highly dependent on the synthetic approach; even though the monoclinic phase[18,59] is mainly observed through solid-state synthesis, metastable phases like cubic are mainly achieved through low-temperature solution-based methods.[23,58,60,61] The annealed $NaSbS_2$ powder was mostly agglomerated in large clusters with elemental constituents homogenously distributed within the compound (Fig. S15†).

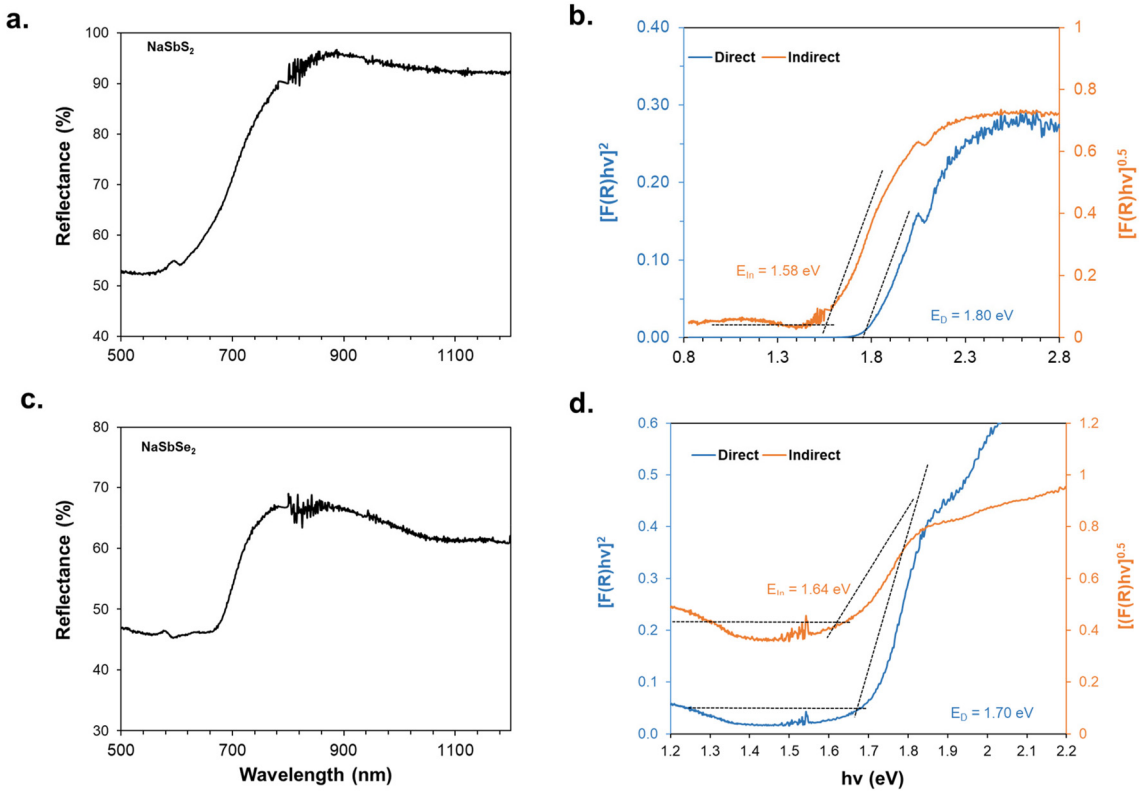

Fig. 8 Solid-state optical diffuse reflectance spectra of (a) $NaSbS_2$, and (c) $NaSbSe_2$, and calculated direct and indirect band gaps from Tauc plots of (b) $NaSbS_2$, and (d) $NaSbSe_2$ compounds.

Alternatively, the generalized form of one-pot reaction scheme for selenides analogs is suggested in eqn (13):

$$2NaHSe_{(sol)} + PnBr_{3(sol)} + 2NaOH_{(sol)} \rightarrow NaPnSe_{2(s)} + 3NaBr_{(sol)} + 2H_2O_{(l)} \quad (Pn = Bi, Sb) \quad (13)$$

Previously, we showed that $NaSbSe_2$ is the main impurity in Na_3SbSe_4 synthesis and is formed even without any NaOH precursor (Fig. S9†) with [Se] : [Sb] = 4 : 1 stoichiometry. Here, we shifted toward phase-pure $NaSbSe_2$ synthesis based on eqn (13) which requires lower Se content. Our preliminary experiments showed that the choice of Se precursor solutions (A or B) does not have any meaningful impact on $NaSbSe_2$ purity. Hence, all the following experiments were carried out with A (clear) solution. Fig. 7c displays the XRD patterns of $NaSbSe_2$ products recovered from ethanolic solution at RT and further annealed at 300 °C. The highly pure $NaSbSe_2$ sample adopts an $Fm\bar{3}m$ cubic structure with $a = c = 5.9914$ Å matching previous reports.[5,62] Similar to other antimony-based chalcogenides, $NaSbSe_2$ is highly crystalline at RT with extra annealing promotes its crystallinity. EDAX mapping further confirmed the purity of the 112 phase (Fig. S16†). In ESI,† we have presented our attempts to extend a similar methodology to synthesize phase-pure $NaBiCh_2$. Table S2† summarizes all the synthetic conditions and parameters used for $NaPnCh_2$ compounds. To investigate the potential of these ternary chalcogenides as candidates for solar energy conversion applications, diffuse reflectance spectroscopy was conducted to measure their optical bandgaps. As shown in Fig. 8, the onset of absorption for $NaSbCh_2$ (Ch = S, Se) compounds begins around 800 nm. In the corresponding Tauc plots, the region with a linear increase in light absorption represents the characteristic of a semiconductor, and the *x*-axis intercept is used for band gap estimation.[63] Both direct and indirect band gaps have been predicted and experimentally measured for $NaSbCh_2$ [23,61] compounds. The direct band gaps calculated for $NaSbS_2$ ($Fm\bar{3}m$) and $NaSbSe_2$ are 1.8 and 1.71 eV, while the indirect transition resulted in 1.58, and 1.64 eV, respectively. These values are in close agreement with the previous reports for nanocrystalline $NaSbS_2$ ($Fm\bar{3}m$) and $NaSbSe_2$ materials.[19,20,23,28]

Conclusions

In this work, we developed simple, solution-based protocols to produce sodium metal chalcogenides used in energy conversion and storage applications. Utilizing ethanolic solutions of activated chalcogens, we synthesized phase-pure Na_3SbCh_4 (Ch = S, Se) and $NaPnCh_2$ (Pn = Sb, Bi, Ch = S, Se) compounds through reactive precipitation at RT with careful precursors selection and reaction optimization. Throughout this work, we observed that the underlying chemistry of chalcogen precursor and solvent interactions directly impact the phase purity of various ternary chalcogenides. Complementary analysis of the XRD and Raman spectroscopy was employed to shed light on the formation of the transient phases and the impact of precursor stoichiometry. Specifically, we identified the pivotal role of NaOH in enabling the redox mechanism of Sb(III) and Sb(V) in the Na_3SbSe_4 formation. Synthesis of the sulfide compound achieved a high yield of 92–95% with ~99 wt% purity whereas the selenide reactions resulted in a lower yield of 74–79% (97.5–99.6 wt% purity). Electrochemical characterization of Na_3SbCh_4 compounds *via* impedance spectroscopy and chronoamperometry demonstrated high ionic conductivity (0.17–0.3 mS cm^{-1}) as well as infinitesimal electronic conductivity further confirming their potential as solid-state electrolytes. Moreover, the one-pot protocol was extended to $NaPnCh_2$ composition and resulted in highly pure ternaries with promising optical properties confirmed through diffuse reflectance UV-Vis spectroscopy. Although the one-pot solution presented in this study does not allow for precise control over the morphology or size of the chalcogenides, it is more scalable compared to other solution-based methods like solvothermal and colloidal hot injection, making it potentially more suitable for large-scale applications.

Author contributions

The manuscript was written through the contributions of all authors. All authors have approved the final version of the manuscript.

Data availability

The data supporting this article have been included as part of the ESI.†

Conflicts of interest

There are no conflicts to declare.

Acknowledgements

We would like to sincerely thank Dr Yuan Yang for her assistance with NMR studies. This work was supported by the National Science Foundation through award 2219184. Some of the work was performed in the following core facility, which is a part of Colorado School of Mines' Shared Instrumentation Facility (X-ray Diffraction & Computed Tomography: RRID: SCR_022053, Scanning Probe and Optical Microscopy: RRID: SCR_022048).

References

1 M. G. Kanatzidis, Discovery-Synthesis, Design, and Prediction of Chalcogenide Phases, *Inorg. Chem.*, 2017, **56**, 3158–3173.

2 M. G. Kanatzidis and S. P. Huang, Coordination chemistry of heavy polychalcogenide ligands, *Coord. Chem. Rev.*, 1994, **130**, 509–621.
3 W. S. Sheldrick and M. Wachhold, Chalcogenidometalates of the heavier Group 14 and 15 elements, *Coord. Chem. Rev.*, 1998, **176**, 211–322.
4 G. W. Drake and J. W. Kolis, The chemistry of mixed 15 16 main group clusters, *Coord. Chem. Rev.*, 1994, **137**, 131–178.
5 N. Kapuria, B. Nan, T. E. Adegoke, U. Bangert, A. Cabot, S. Singh and K. M. Ryan, Colloidal Synthesis of Multinary Alkali-Metal Chalcogenides Containing Bi and Sb: An Emerging Class of I–V–VI 2 Nanocrystals with Tunable Composition and Interesting Properties, *Chem. Mater.*, 2023, **35**, 4810–4820.
6 H. McKeever, N. N. Patil, M. Palabathuni and S. Singh, Functional Alkali Metal-Based Ternary Chalcogenides: Design, Properties, and Opportunities, *Chem. Mater.*, 2023, **35**, 9833–9846.
7 F. Strauss, J. H. Teo, J. Janek and T. Brezesinski, Investigations into the superionic glass phase of Li4PS4I for improving the stability of high-loading all-solid-state batteries, *Inorg. Chem. Front.*, 2020, **7**, 3953–3960.
8 N. Zhao, D. Lu, J. Xu, K. Wu, H. Yu and H. Zhang, Greatly enhanced optical anisotropy in thiophosphates inspired by rational coupling of tetrahedra and ethane-like [P2S6]4– groups, *Inorg. Chem. Front.*, 2024, **11**, 4603–4610.
9 H. Jia, L. Peng, C. Yu, L. Dong, S. Cheng and J. Xie, Chalcogenide-based inorganic sodium solid electrolytes, *J. Mater. Chem. A*, 2021, 5134–5148.
10 Y. Tian, T. Shi, W. D. Richards, J. Li, J. C. Kim, S.-H. Bo and G. Ceder, Compatibility issues between electrodes and electrolytes in solid-state batteries, *Energy Environ. Sci.*, 2017, **10**, 1150–1166.
11 S. A. Vaselabadi, K. Palmer, W. H. Smith and C. A. Wolden, Scalable Synthesis of Selenide Solid-State Electrolytes for Sodium-Ion Batteries, *Inorg. Chem.*, 2023, **62**, 17102–17114.
12 S. A. Vaselabadi, W. H. Smith and C. A. Wolden, Solution Synthesis of Sb2S3 and Na3SbS4 Solid-State Electrolyte, *J. Electrochem. Soc.*, 2021, **168**, 110533.
13 Y. Yang, S. Yang, X. Xue, X. Zhang, Q. Li, Y. Yao, X. Rui, H. Pan and Y. Yu, Inorganic All–Solid–State Sodium Batteries: Electrolyte Designing and Interface Engineering, *Adv. Mater.*, 2023, **2308332**, 1–24.
14 J. Huang, K. Wu, G. Xu, M. Wu, S. Dou and C. Wu, Recent progress and strategic perspectives of inorganic solid electrolytes: fundamentals, modifications, and applications in sodium metal batteries, *Chem. Soc. Rev.*, 2023, 4933–4995.
15 O. Maus, M. T. Agne, T. Fuchs, P. S. Till, B. Wankmiller, J. M. Gerdes, R. Sharma, M. Heere, N. Jalarvo, O. Yaffe, M. R. Hansen and W. G. Zeier, On the Discrepancy between Local and Average Structure in the Fast Na + Ionic Conductor Na2.9Sb0.9W0.1S4, *J. Am. Chem. Soc.*, 2023, **145**, 7147–7158.
16 R. McClain, C. D. Malliakas, J. Shen, J. He, C. Wolverton, G. B. González and M. G. Kanatzidis, Mechanistic insight of KBiQ2(Q = S, Se) using panoramic synthesis towards synthesis-by-design, *Chem. Sci.*, 2021, **12**, 1378–1391.
17 B. A. Aragaw, J. Sun, D. J. Singh and M. W. Lee, Ion exchange-prepared NaSbSe2 nanocrystals: Electronic structure and photovoltaic properties of a new solar absorber material, *RSC Adv.*, 2017, **7**, 45470–45477.
18 W. W. W. Leung, C. N. Savory, R. G. Palgrave and D. O. Scanlon, An experimental and theoretical study into NaSbS2 as an emerging solar absorber, *J. Mater. Chem. C*, 2019, **7**, 2059–2067.
19 A. Baqais, N. Tymińska, T. Le Bahers and K. Takanabe, Optoelectronic Structure and Photocatalytic Applications of Na(Bi,La)S 2 Solid Solutions with Tunable Band Gaps, *Chem. Mater.*, 2019, **31**, 3211–3220.
20 B. A. Rosales, M. A. White and J. Vela, Solution-Grown Sodium Bismuth Dichalcogenides: Toward Earth-Abundant, Biocompatible Semiconductors, *J. Am. Chem. Soc.*, 2018, **140**, 3736–3742.
21 A. M. Medina-Gonzalez, B. A. Rosales, U. H. Hamdeh, M. G. Panthani and J. Vela, Surface Chemistry of Ternary Nanocrystals: Engineering the Deposition of Conductive NaBiS2 Films, *Chem. Mater.*, 2020, **32**, 6085–6096.
22 T. J. Slade, J. A. Grovogui, J. J. Kuo, S. Anand, T. P. Bailey, M. Wood, C. Uher, G. J. Snyder, V. P. Dravid and M. G. Kanatzidis, Understanding the thermally activated charge transport in NaPbMSbQm +2(Q = S, Se, Te) thermoelectrics: Weak dielectric screening leads to grain boundary dominated charge carrier scattering, *Energy Environ. Sci.*, 2020, **13**, 1509–1518.
23 A. M. Medina-Gonzalez, P. Yox, Y. Chen, M. A. S. Adamson, B. A. Rosales, M. Svay, E. A. Smith, R. D. Schaller, K. Wu, A. J. Rossini, K. Kovnir and J. Vela, Solution-Grown Ternary Semiconductors: Nanostructuring and Stereoelectronic Lone Pair Distortions in I–V–VI 2 Materials, *Chem. Mater.*, 2022, **34**, 7357–7368.
24 I. S. Khare, N. J. Szymanski, D. Gall and R. E. Irving, Electronic, optical, and thermoelectric properties of sodium pnictogen chalcogenides: A first principles study, *Comput. Mater. Sci.*, 2020, **183**, 109818.
25 X. Liu, N. Fechler and M. Antonietti, Salt melt synthesis of ceramics, semiconductors and carbon nanostructures, *Chem. Soc. Rev.*, 2013, **42**, 8237–8265.
26 W. S. Sheldrick and M. Wachhold, Solventothermal Synthesis of Solid–State Chalcogenidometalates, *Angew. Chem., Int. Ed. Engl.*, 1997, **36**, 206–224.
27 H. Fei, Z. Feng and X. Liu, Novel sodium bismuth sulfide nanostructures: a promising anode materials for sodium-ion batteries with high capacity, *Ionics*, 2015, **21**, 1967–1972.
28 P. Rong, S. Gao, H. Lu, S. Ren, M. Zhang, S. Jiao, Y. Zhang and J. Wang, Hierarchical Nanosheet-Based NaBiS2 Flowers for High-Performance and Self-Powered Broadband Photodetectors, *ACS Appl. Nano Mater.*, 2022, **5**, 11003–11010.
29 S. Kang, Y. Hong and Y. Jeon, A facile synthesis and characterization of sodium bismuth sulfide (NaBiS2) under

hydrothermal condition, *Bull. Korean Chem. Soc.*, 2014, **35**, 1887–1890.

30 R. B. Zheng, J. H. Zeng, M. S. Mo and Y. T. Qian, Solvothermal synthesis of the ternary semiconductor AInS2 (A = Na, K) nanocrystal at low temperature, *Mater. Chem. Phys.*, 2003, **82**, 116–119.

31 V. G. Dileepkumar, P. S. Surya, C. Pratapkumar, R. Viswanatha, C. R. Ravikumar, M. R. Anil Kumar, H. B. Muralidhara, I. M. Al-Akraa, A. M. Mohammad, Z. Chen, X.-T. Bui and M. S. Santosh, NaFeS2 as a new photocatalytic material for the degradation of industrial dyes, *J. Environ. Chem. Eng.*, 2020, **8**, 104005.

32 J. F. W. Mosselmans, G. R. Helz, R. A. D. Pattrick, J. M. Charnock and D. J. Vaughan, A study of speciation of Sb in bisulfide solutions by X-ray absorption spectroscopy, *Appl. Geochem.*, 2000, **15**, 879–889.

33 W. H. Smith, J. Birnbaum and C. A. Wolden, Production and purification of anhydrous sodium sulfide, *J. Sulfur Chem.*, 2021, **42**, 426–442.

34 X. Yang, Q. Wang, Y. Tao and H. Xu, A Modified Method to Prepare Diselenides by the Reaction of Selenium with Sodium Borohydride, *J. Chem. Res.*, 2002, **2002**, 160–161.

35 B. H. Toby and R. B. Von Dreele, GSAS-II : the genesis of a modern open-source all purpose crystallography software package, *J. Appl. Crystallogr.*, 2013, **46**, 544–549.

36 D. Xu, S. Shen, Y. Zhang, H. Gu and Q. Wang, Selective Synthesis of Ternary Copper–Antimony Sulfide Nanocrystals, *Inorg. Chem.*, 2013, **52**, 12958–12962.

37 P. Kubelka and F. Munk, An article on optics of paint layers, *Tech. Phys.*, 1931, 1–16.

38 A. V. Kurzin, A. N. Evdokimov, V. S. Golikova and O. S. Pavlova, Solubility of sodium sulfide in alcohols, *J. Chem. Eng. Data*, 2010, **55**, 4080–4081.

39 W. H. Smith, S. A. Vaselabadi and C. A. Wolden, Synthesis of high-purity Li2S nanocrystals via metathesis for solid-state electrolyte applications, *J. Mater. Chem. A*, 2023, **11**, 7652–7661.

40 S. P. Pinho and E. A. Macedo, Solubility of NaCl, NaBr, and KCl in water, methanol, ethanol, and their mixed solvents, *J. Chem. Eng. Data*, 2005, **50**, 29–32.

41 L. Zhang, D. Zhang, K. Yang, X. Yan, L. Wang, J. Mi, B. Xu and Y. Li, Vacancy–Contained Tetragonal Na3SbS4 Superionic Conductor, *Adv. Sci.*, 2016, **3**, 1600089.

42 W. Mikenda and A. Preisinger, Vibrational spectra of Na3SbS4, Na3SbS4·9H_2O (Schlippe's salt) and Na3SbS4·9D_2O, *Spectrochim. Acta, Part A*, 1980, **36**, 365–370.

43 H. C. Brown, E. J. Mead and B. C. Subba Rao, A Study of Solvents for Sodium Borohydride and the Effect of Solvent and the Metal Ion on Borohydride Reductions 1, *J. Am. Chem. Soc.*, 1955, **77**, 6209–6213.

44 D. L. Klayman and T. S. Griffin, Reaction of Selenium with Sodium Borohydride in Protic Solvents. A Facile Method for the Introduction of Selenium into Organic Molecules, *J. Am. Chem. Soc.*, 1973, **95**, 197–199.

45 S. Ganguli, S. Ghosh, G. Tudu, H. V. S. R. M. Koppisetti and V. Mahalingam, Design Principle of Monoclinic NiCo2Se4 and Co3Se4 Nanoparticles with Opposing Intrinsic and Geometric Electrocatalytic Activity toward the OER, *Inorg. Chem.*, 2021, **60**, 9542–9551.

46 U. K. Gautam, M. Nath and C. N. R. Rao, New strategies for the synthesis of t-selenium nanorods and nanowires, *J. Mater. Chem.*, 2003, **13**, 2845–2847.

47 A. R. M. De Oliveira, L. Piovan, F. Simonelli, A. Barison, M. D. F. C. Santos and M. B. M. De Mello, A77Se NMR study of elemental selenium reduction using NaBH4, *J. Organomet. Chem.*, 2016, **806**, 54–59.

48 J. D. Odom, W. H. Dawson and P. D. Ellis, Selenium-77 Relaxation Time Studies on Compounds of Biological Importance: Dialkyl Selenides, Dialkyl Diselenides, Selenols, Selenonium Compounds, and Seleno Oxyacids, *J. Am. Chem. Soc.*, 1979, **101**, 5815–5822.

49 J. Cusick and I. Dance, The characterization of [HSe]- and [Sex]2- ions by 77Se NMR, *Polyhedron*, 1991, **10**, 2629–2640.

50 M. Bjoergvinsson and G. J. Schrobilgen, Homo- and heteropolychalcogenide anions Ch2-, HCh-, Ch22-, $Ch_3$2-, and Ch42- (Ch = selenium and/or tellurium): solution proton, selenium-77, tellurium-123 and -125 NMR study, *Inorg. Chem.*, 1991, **30**, 2540–2547.

51 Y. Abusa, P. Yox, S. D. Cady, G. Viswanathan, J. Opare-addo, E. A. Smith, Y. Mudryk, O. I. Lebedev, A. Perras, K. Kovnir, F. A. Perras and K. Kovnir, Make Selenium Reactive Again: Activating Elemental Selenium for Synthesis of Metal Selenides Ranging from Nanocrystals to Large Single Crystals, *J. Am. Chem. Soc.*, 2023, **145**, 22762–22775.

52 C. T. Irvine, N. Hoefer, M. J. Moser, R. A. Nelson, D. W. McComb and J. E. Goldberger, Diselenide Dianion's Dual Powers: PdSe2 Polymorph Control and Pd3Se10 Superatomic Crystal Creation, *Chem. Mater.*, 2023, **35**, 4404–4411.

53 F. Baum, T. Pretto, A. G. Brolo and M. J. L. Santos, Uncovering the Mechanism for the Formation of Copper Thioantimonate (SbV) Nanoparticles and Its Transition to Thioantimonide (SbIII), *Cryst. Growth Des.*, 2018, **18**, 6521–6527.

54 P. Till, M. T. Agne, M. A. Kraft, M. Courty, T. Famprikis, M. Ghidiu, T. Krauskopf, C. Masquelier and W. G. Zeier, Two-Dimensional Substitution Series Na3P1−xSbxS4−ySey : Beyond Static Description of Structural Bottlenecks for Na + Transport, *Chem. Mater.*, 2022, **34**, 2410–2421.

55 S. Xiong, Z. Liu, H. Rong, H. Wang, M. McDaniel and H. Chen, Na3SbSe4-xSx as Sodium Superionic Conductors, *Sci. Rep.*, 2018, **8**, 2–8.

56 A. Banerjee, K. H. Park, J. W. Heo, Y. J. Nam, C. K. Moon, S. M. Oh, S.-T. T. Hong and Y. S. Jung, Na3SbS4: A Solution Processable Sodium Superionic Conductor for All-Solid-State Sodium-Ion Batteries, *Angew. Chem., Int. Ed.*, 2016, **55**, 9634–9638.

57 H. Wang, Y. Chen, Z. D. Hood, G. Sahu, A. S. Pandian, J. K. Keum, K. An and C. Liang, An Air-Stable Na3SbS4 Superionic Conductor Prepared by a Rapid and Economic Synthetic Procedure, *Angew. Chem., Int. Ed.*, 2016, **55**, 8551–8555.

58 Z. Xia, F. X. Yu, S. C. Lu, D. J. Xue, Y. S. He, B. Yang, C. Wang, R. Q. Ding, J. Zhong and J. Tang, Synthesis and characterization of NaSbS2 thin film for potential photodetector and photovoltaic application, *Chin. Chem. Lett.*, 2017, **28**, 881–887.

59 V. A. Bazakutsa, N. I. Gnidash, A. K. Kul'chitskaya and A. V. Salov, Photoelectric and optical properties of thin films of ternary chalcogenides of the form MeISbX2VI, *Sov. Phys. J.*, 1975, **18**, 472–475.

60 M. Zubair, S. A. Ahad, I. S. Amiinu, V. A. Lebedev, M. Mishra, H. Geaney, S. Singh and K. M. Ryan, Colloidal synthesis of the mixed ionic-electronic conducting NaSbS2 nanocrystals, *Nanoscale Horiz.*, 2023, **8**, 1262–1272.

61 P. C. Harikesh, A. Surendran, B. Ghosh, R. A. John, A. Moorthy, N. Yantara, T. Salim, K. Thirumal, W. L. Leong, S. Mhaisalkar and N. Mathews, Cubic NaSbS2 as an Ionic–Electronic Coupled Semiconductor for Switchable Photovoltaic and Neuromorphic Device Applications, *Adv. Mater.*, 2020, **32**, 1–9.

62 B. Eisenmann and H. Schäfer, Über Seleno– und Telluroarsenite, –antimonite und –bismutite, *Z. Anorg. Allg. Chem.*, 1979, **456**, 87–94.

63 P. Makuła, M. Pacia and W. Macyk, How To Correctly Determine the Band Gap Energy of Modified Semiconductor Photocatalysts Based on UV–Vis Spectra, *J. Phys. Chem. Lett.*, 2018, **9**, 6814–6817.